

Exploring the low-energy landscape of large-scale signed social networks

G. Facchetti, G. Iacono, and C. Altafini*

SISSA, via Bonomea 265, 34136 Trieste, Italy

(Received 1 June 2012; published 26 September 2012)

Analogously to a spin glass, a large-scale signed social network is characterized by the presence of disorder, expressed in this context (and in the social network literature) by the concept of structural balance. If, as we have recently shown, the signed social networks currently available have a limited amount of true disorder (or frustration), it is also interesting to investigate how this frustration is organized, by exploring the landscape of near-optimal structural balance. What we obtain in this paper is that while one of the networks analyzed shows a unique valley of minima, and a funneled landscape that gradually and smoothly worsens as we move away from the optimum, another network shows instead several distinct valleys of optimal or near-optimal structural balance, separated by energy barriers determined by internally balanced subcommunities of users, a phenomenon similar to the replica-symmetry breaking of spin glasses. Multiple, essentially isoenergetic, arrangements of these communities are possible. Passing from one valley to another requires one to destroy the internal arrangement of these balanced subcommunities and then to reform it again. It is essentially this process of breaking the internal balance of the subcommunities which gives rise to the energy barriers.

DOI: [10.1103/PhysRevE.86.036116](https://doi.org/10.1103/PhysRevE.86.036116)

PACS number(s): 89.75.Fb, 75.10.Nr, 89.20.Hh

I. INTRODUCTION

Signed social networks represent an interesting class of networks at the interface between network theory, social sciences, and statistical physics [1–7]. In these networks, the nodes represent the individuals and the edges can assume a positive or a negative sign according to the type of relationship established between pairs of individuals: a positive edge represents a form of friendship-collaboration-trust (“I like”), while a negative edge represents aversion-competition-mistrust (“don’t like”).

Like in an Ising spin glass, the presence of negative edges introduces frustration in the network, which for social networks is associated to a property called structural balance, introduced by Heider in [8], then generalized and formulated in graphical terms by Cartwright-Harary in [9]. According to the theory proposed by Heider, individuals tend to establish relations that avoid tensions: this can be condensed in the statement “*the enemy of my enemy is my friend*” (and similar, equivalent statements; see, e.g., Fig. 1 of [2]). When these social interactions are described through signed networks, the theory can be reformulated in terms of frustration of the cycles which are present in the corresponding signed graphs [9]. In particular, all cycles with an odd number of negative edges (hereafter called negative cycles) are frustrated: they do not obey Heider’s principle and they contribute to the global frustration of the whole network. Since the concept of frustration is formally identical to the one used in spin glass theory [10], also the notion of structural balance admits a statistical physics analog. Exact structural balance, in particular, corresponds to lack of frustration, as in a Mattis model [11].

In this model the negative edges form only positive cycles, and hence the disorder they introduce into the system is only apparent and can be completely eliminated by equivalence transformations called gauge transformations [12]. On the contrary, the frustration cannot be eliminated by equivalence

transformations; hence it is sometimes referred to as true disorder.

In the general case, computing the structural balance of a signed social network corresponds to computing the ground state of a (nonplanar) Ising spin glass, which is a well-known NP-hard problem [13,14]. In fact, in social network theory a common approach to overcome this difficulty has been to focus on the simplest cyclic motif potentially encoding frustration, namely triangles of pairwise relations, comparing the frequency of positive and negative triangles [7,15]. However, the determination of the level of balance cannot always be reduced to the count and characterization of local motifs. If for all-to-all networks [1,5] triangles are a reliable measure of structural balance, for heterogeneous networks (like real social networks) it is not clear to what extent counting triangles reflects the structural balance (which is a global property [6], in the Cartwright-Harary generalization).

For this purpose, in [2], exploiting the analogy between signed social networks and Ising spin glasses we have computed structural balance using algorithms inspired by the literature on ground state search. On the signed social networks currently available (which can reach sizes of 10^5 nodes), these calculations have proved quite effective (with a guaranteed precision of 5% in the value of structural balance), and have allowed one to conclude that these networks are extremely balanced, much more than expected from random edge sign distributions. In spin glass terminology, this result can be restated by saying that the social networks have a limited amount of true disorder (or frustration) and a significant amount of apparent disorder.

The algorithm we have used (described in some detail in [2]; see also [16]) has an heuristic character, hence in order to obtain reliable results it has to be run many times, changing the initial conditions and the random seeds. In statistical physics terminology, each such run corresponds to a replica of the system. As the “cooling” schedule differs from replica to replica, the level of structural balance, i.e., the energy reached (which typically corresponds to a local minimum), may differ from one replica to the other.

*Corresponding author: altafini@sissa.it

The purpose of this paper is to use the large amount of independent replicas produced in this way to try to obtain a description of the low-energy landscape of the system, i.e., of the landscape of near optimal balance of the social networks. In statistical physics, in the presence of frustration the low-energy landscape is usually rugged and contains a lot of useful information on the properties of the spin glass. For example, if the system has multiple distinct valleys of nearly identical energy separated by energetic barriers, then it is said to have a replica symmetry breaking picture [17], meaning that ergodicity is broken and different cooling procedures lead to different, isoenergetic (or nearly isoenergetic), minima separated by energy barriers. Some other times, instead, it may happen that the landscape is funneled around a single “dominant” valley, possibly surrounded by a plethora of local minima of little significance (and progressively higher energy). The two different pictures are both observed on the two social networks considered in this study. Most interestingly, we can also obtain insight on the origin of these differences in the landscape. In the case of multiple competing valleys, in fact, it is possible to isolate internally balanced subcommunities whose orientation with respect to the rest of the network changes passing from one valley to another. The sample paths connecting one valley to the other require one to destroy the internal balance of (some of) these subcommunities and then to reform it again in the opposite orientation. It appears that the energy barriers between the near-optimal valleys is largely due to this process of breaking the internal balance of the subcommunities. In the case of funneled landscape, no internally balanced subcommunity can instead be observed. In any case, in both pictures all low-energy replicas are sufficiently close to each other, a situation which corresponds to a “partially ferromagnetic” spin glass, coherently with the large fraction of positive edges, as well as with the low frustration that characterizes these networks.

II. SIGNED SOCIAL NETWORKS AND THEIR STRUCTURAL BALANCE

In this work we consider the following two signed social networks:

- (i) *Epinions*: trust-distrust network among users of product review website Epinions [15,18].
- (ii) *Slashdot*: friend-foes network of the technological news site Slashdot (Zoo feature) [19,20].

Both are downloadable from the Stanford Network Analysis Platform (<http://snap.stanford.edu/>). Numbers of nodes (n), edges (m), and edge signs are provided in Table I, where we report also the data for the largest two-component subnetwork on which all the analysis has been performed. Indeed, leaves can be removed since they are not involved in cycles, hence they do not contribute to frustration. Further details on these networks are provided in [15]; see also [20] for Slashdot.

Call $\mathbf{s} = [s_1 \dots s_n]^T$ with $s_i \in \{\pm 1\} = \mathbb{B}_2$, $i = 1, \dots, n$, the “spin” variables associated to the nodes (individuals) of the network. Let also \mathcal{J} be the $n \times n$ symmetric matrix of entries J_{ij} which represent the undirected relationships between nodes s_i and s_j (friendship: $J_{ij} = +1$; hostility: $J_{ij} = -1$). Computing the global structural balance means assigning a +1 or a -1 to the nodes in such a way as to minimize the

TABLE I. Social networks. Main features of the two networks: n and m are the number of nodes and edges of the undirected graph. The two-component subnetwork has been obtained considering only the largest connected component and removing all leaves. In this paper relationships are always represented as mutual, i.e., the edges are undirected.

Network	Original network				
	n	m	No. of –	No. of +	
<i>Epinions</i>	131828	841372	123705	717667	
<i>Slashdot</i>	82144	549202	124130	425072	
Largest two-component subnetwork					
Network	n	m	No. of –	No. of +	%–
<i>Epinions</i>	59235	641734	106286	535448	16.5
<i>Slashdot</i>	52048	468523	112023	356500	23.9

energy function:

$$h(\mathbf{s}) = \sum_{(i,j)} (1 - J_{ij}s_i s_j)/2, \quad (1)$$

where the summation runs over all adjacent pairs of nodes. In matrix form (1) is

$$h(\mathbf{s}) = m - \frac{1}{2} \mathbf{s}^T \mathcal{J} \mathbf{s}.$$

The network is exactly balanced when there exists $\mathbf{s} \in \mathbb{B}_2^n$ such that all terms in (1) can be made simultaneously equal to zero. If this is not the case, then global balance becomes the solution of a Boolean optimization problem,

$$\delta = \min_{\mathbf{s} \in \mathbb{B}_2^n} h(\mathbf{s}) = \min_{\mathbf{s} \in \mathbb{B}_2^n} (m - \frac{1}{2} \mathbf{s}^T \mathcal{J} \mathbf{s}). \quad (2)$$

In correspondence of $\mathbf{s}_o = \text{argmin}_{\mathbf{s} \in \mathbb{B}_2^n} h(\mathbf{s})$, the residual positive terms in (1) correspond to the least number of unbalanced pairwise relationships between nodes [i.e., the frustrations of the spin glass Hamiltonian (1) in its ground state].

For the networks considered in this study an heuristic estimate of δ was carried out in [2]. Recall from [2] that the algorithm we apply uses the idea of gauge transformations as a way to progressively eliminate the apparent disorder in the adjacency matrix \mathcal{J} ; see [2] for the details. The outcome of the algorithm is a gauge-equivalent adjacency matrix $\mathcal{J}_\sigma = T_\sigma \mathcal{J} T_\sigma$, where the diagonal matrix $T_\sigma = \text{diag}(\sigma)$, $\sigma = [\sigma_1, \dots, \sigma_n]$, $\sigma_i = \pm 1$, is chosen so as to minimize the number of negative entries of \mathcal{J}_σ (transformations $\mathcal{J} \rightarrow \mathcal{J}_\sigma$ are called gauge transformations in the statistical physics literature [12]). The practical (iterative) heuristic construction of T_σ is explained in the Supplementary Notes of [2].

The optimization procedure is repeated many times, starting from different initial points (independently and randomly chosen). Denote $\delta_{\text{up}} = \min_k \delta^{(k)}$ the best estimate obtained for the ground state energy over all replicas. Consider an energy band of width ϵ above δ_{up} . For both networks $\epsilon/\delta_{\text{up}} \sim 0.6\%$ is chosen, meaning a few hundreds of energy levels above δ_{up} are considered; see Table II. Only replicas reaching the interval $[\delta_{\text{up}}, \delta_{\text{up}} + \epsilon]$ are retained for further analysis. The number of such replicas is $r = 606$ for Epinions and $r = 5557$ for Slashdot; see Table II. The tight gap between the lower (δ_{low})

TABLE II. Structural balance. For the networks of Table I, we report a lower and an upper bound (δ_{low} and δ_{up}) on the true structural balance (data from [2]). The high ratio $\delta_{\text{up}}/\delta_{\text{low}}$ shows that indeed our calculations are approaching sufficiently close the true ground state energy. By construction, $\delta_{\text{up}} = \min_k \delta^{(k)}$ over all replicas considered, and only the r replicas of energy $\delta^{(k)} \in [\delta_{\text{up}}, \delta_{\text{up}} + \epsilon]$ are considered.

	δ_{low}	δ_{up}	$\delta_{\text{up}}/\delta_{\text{low}}$	ϵ	r
<i>Epinions</i>	50452	50806	0.9930	310	606
<i>Slashdot</i>	70014	73604	0.9512	450	5557

and upper (δ_{up}) estimate for δ (see Table II) guarantees that these replicas are indeed low-energy minima sufficiently close to the true value of structural balance.

The histogram of the values of energies and the (relative) Hamming distances between these minima are reported respectively in Fig. 1 and in Fig. 2 for the two networks. A first comparison of these energies shows a significant difference between the two networks: the histogram for *Epinions* reports only a single broad group, whereas the histogram for *Slashdot* shows three peaks; see Fig. 1. If we compute the relative Hamming distances between each pair of replicas (see Fig. 2), the two networks still present a different behavior: for *Epinions* the minima are all close one to the other (Hamming distances are distributed like a single Gaussian peak); on the contrary, several peaks can be identified among the minima we have found for *Slashdot*.

It is worth noting that, since the energy has a global spin flip symmetry [i.e., $h(\mathbf{s}) = h(-\mathbf{s})$], the Hamming distances $d(\mathbf{s}^{(1)}, \mathbf{s}^{(2)})$ and $d(\mathbf{s}^{(1)}, -\mathbf{s}^{(2)})$ are not distinguishable. This amounts to saying that only relative distances between 0 and

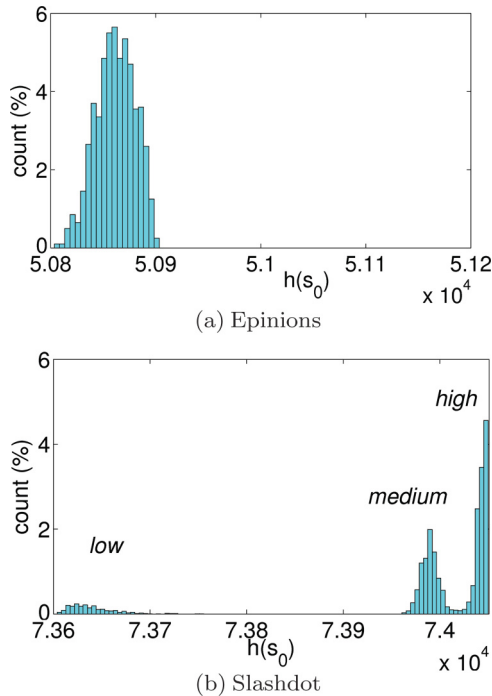


FIG. 1. (Color online) Distribution of the energies for all near-optimal replicas. The leftmost bar of each histogram corresponds to δ_{up} .

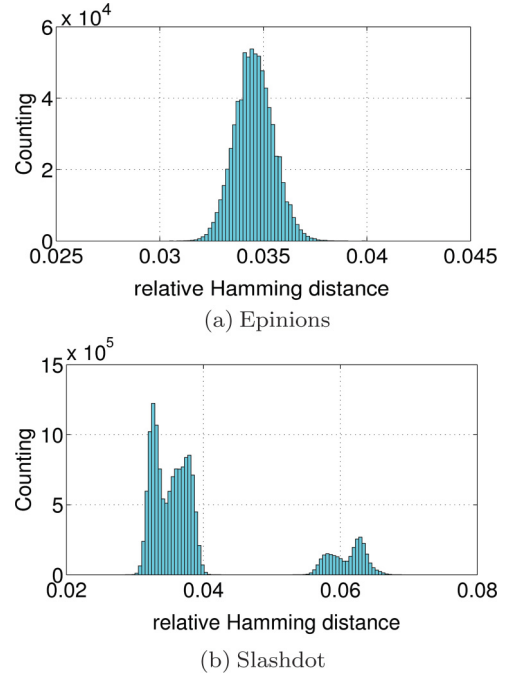


FIG. 2. (Color online) Relative Hamming distance between low-energy replicas.

1/2 can be considered (analogously to the Ising spin glass case). We follow this principle throughout the paper.

III. COMPUTATION OF THE LOW-ENERGY SPIN PATTERNS

Since we can expect that each replica represents a different local minimum in the energy landscape, we can explore the distribution of the frequencies of the sign with which a spin appears in the r replicas: in particular, if $\mathbf{s}^{(1)}, \dots, \mathbf{s}^{(r)}$ are the configuration states of the minima in the r replicas, for each spin i we can define

$$v_i = \frac{1}{r} \min \left\{ \sum_{k=1}^r \frac{1 - s_i^{(k)}}{2}, \sum_{k=1}^r \frac{s_i^{(k)} + 1}{2} \right\},$$

where the two ratios represent the number of replicas in which the i th spin has negative and positive sign, respectively. For each value of v between 0 and 1/2 (the histograms stop at $v = 1/2$ because of the global spin flip symmetry), the subset $W(v)$ of spins which have $v_i = v$ can be identified. For the subgraph corresponding to $W(v)$, we calculate (i) the number of spins $n(v)$, (ii) the number of connected components $c(v)$, and (iii) the maximal size of these connected components $z(v)$.

Exploring the distribution of the frequency index $c(v)$ (see the second panel in each row of Fig. 3), we can observe that both networks have broad peaks around frequencies $v = 1/3$ and $v = 1/2$, meaning that the corresponding spins appear flipped in a half or in a third of the low-energy replicas. The peak at $v = 0$ corresponds to spins with equal orientation in all replicas; hence it constitutes a fixed “backbone” which does not contribute to the variability.

A characterization of the two peaks at $v = 1/2$ and $v = 1/3$ in the plot of the index $c(v)$ can be carried out through a probabilistic model. By construction, the replicas

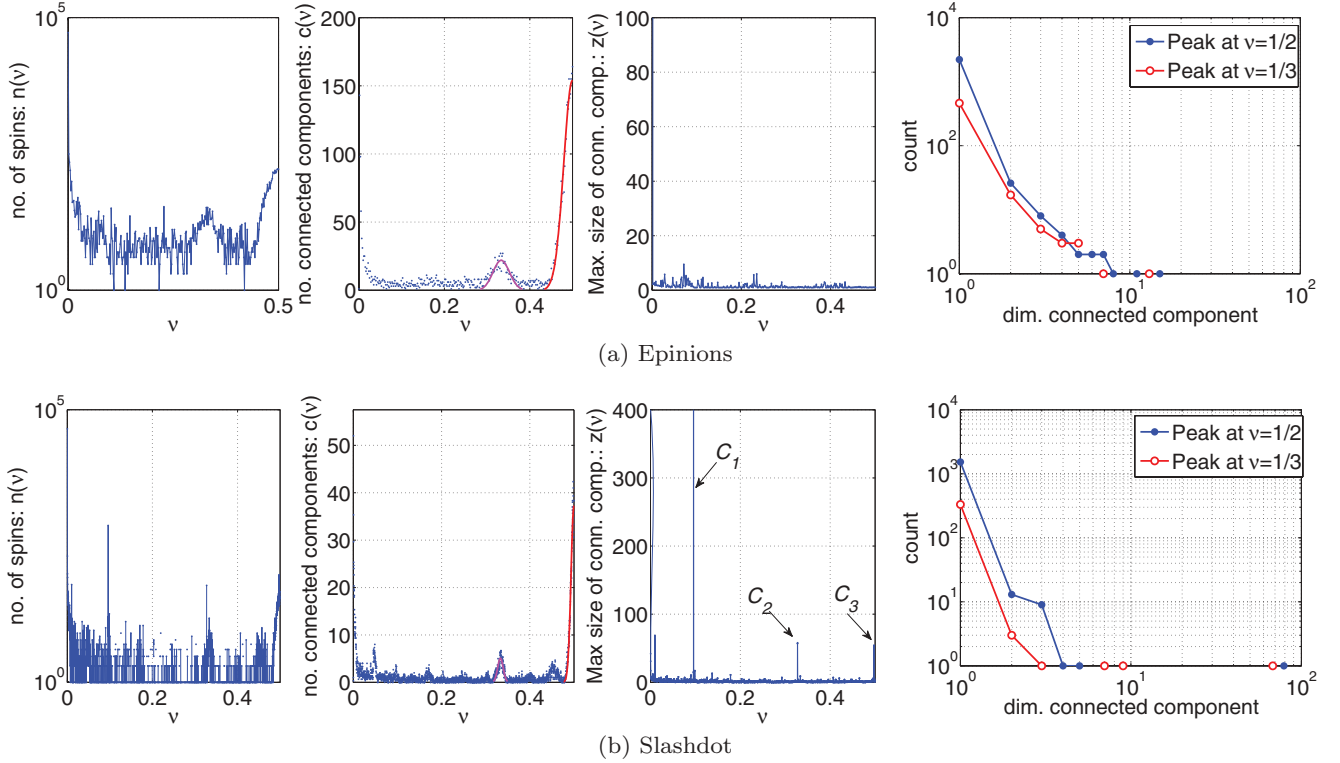


FIG. 3. (Color online) Indices $n(\nu)$, $c(\nu)$, and $z(\nu)$ for the two networks. The rightmost panel in each row reports the dimensions of the connected components identified in the subgraph $W(\nu)$ of spins under the two peaks of $c(\nu)$ centered at $\nu = 1/3$ and at $\nu = 1/2$. Letters C_1 , C_2 , and C_3 indicate the three Slashdot communities identified in the spikes pointed to by the arrows.

are statistically independent. We may also expect that the flipping components which belong to the peak at $\nu = 1/2$ are independent with respect to the flipping components around $\nu = 1/3$ (and vice versa). Under these assumptions, the two peaks can be modeled separately [the plot of $c(\nu)$ is then viewed as the overlap of two curves], considering the binomial probability distribution $B(r, p)$ as the theoretical distribution for the variable $r\nu$ for each peak:

$$\mathbb{P}[r\nu = k] = \binom{r}{k} p^k (1 - p)^{r-k} \quad (3)$$

(where the value of p is fixed at $p = 1/2$ and $p = 1/3$ for the two peaks). If $Y(k)$ is a random variable representing the number of connected components (over a population of q flipping components, q unknown) having $\nu = k/r$, and assuming that each connected component can flip independently, then

$$Y(k) \sim B(q, \mathbb{P}[r\nu = k]).$$

By (3), its expectation value is

$$\mathbb{E}[Y(k)] = q \binom{r}{k} p^k (1 - p)^{r-k},$$

where the parameter q can be obtained by linear regression, fitting the experimental data with k varying inside the support of the peak. Once a level of significance α has been fixed, we can select only spins which are in the central part of the fitted peak with p value less than α , as determined through an hypothesis test. The selected values of ν include only regions where the fitting error is smaller or at least comparable with the root mean square deviation (r.m.s.d.) of the data at each ν .

Extrapolating the connected subgraphs under the two peaks (Table III reports the results of the probabilistic model applied to the interpolation of these peaks), it is

TABLE III. Probabilistic binomial model for the spin frequencies. Parameters of the fitting of the binomial probability distribution to the broad peaks of $c(\nu)$ of spin frequencies $\nu = 1/2$ and $\nu = 1/3$; see Fig. 3 (second panel of each row). Ranges are expressed as relative to the total number of replicas. For Epinions the selected intervals correspond respectively to $\nu \in [0.46, 0.50]$ and $\nu \in [0.31, 0.36]$. For Slashdot, the test yields the intervals $\nu \in [0.49, 0.50]$ and $\nu \in [0.32, 0.34]$.

<i>Epinions</i>		
<i>Parameter</i>	$\nu = 1/2$	$\nu = 1/3$
k/r range for fitting	$[\frac{263}{606}, \frac{303}{606}]$	$[\frac{172}{606}, \frac{232}{606}]$
Fitting parameter q	2378	642
r.m.s.d.	8	4
α	0.05	0.10
Selected region	$[\frac{279}{606}, \frac{303}{606}]$	$[\frac{187}{606}, \frac{217}{606}]$
No. selected components	2336	528
<i>Slashdot</i>		
<i>Parameter</i>	$\nu = 1/2$	$\nu = 1/3$
k/r range for fitting	$[\frac{2648}{5557}, \frac{2778}{5557}]$	$[\frac{1762}{5557}, \frac{1942}{5557}]$
Fitting parameter q	1740	447
r.m.s.d.	3	1
α	0.10	0.10
Selected region	$[\frac{2717}{5557}, \frac{2778}{5557}]$	$[\frac{1807}{5557}, \frac{1897}{5557}]$
No. selected components	1656	419

possible to obtain statistics of the recurrent motifs which form most of the variability of the spin configurations around a ground state. A catalog of isoenergetic motifs (isoenergetic alternatives for a ground state) we identified through this interpolation is provided in Tables VI and VII (see also the Appendix for more detailed characterization of these flipping motifs).

IV. ANALYSIS OF THE LOW-ENERGY LANDSCAPES FOR THE TWO NETWORKS

A. Epinions: A single valley

We can deduce from the histograms of Figs. 1 and 2 that all the minima of the Epinions network belong to the same valley. As we move away from the bottom of the valley (global minimum), the energy tends to grow. This feature can be deduced from the analysis of the distance among replicas versus energy of a replica reported in Fig. 4(a). The two-dimensional bar plot shows that, moving away from the minimum of energy, the Hamming distance increases monotonically. This means that the valley is characterized by sufficiently regular ascending walls, and that the basin of attraction of the global minimum is rather broad.

The high degeneracy of the ground state, which is also suggested by the sample trajectories of Fig. 4(b), is a well-known feature of Ising spin glasses with bimodal bonds [21]. The flipping of the isoenergetic motifs we have identified (see Tables VI and VII and Appendix) may explain the broadening of the distribution of the Hamming distance. Apart from these degeneracies, the Epinions network contains many small disjoint motifs (scattered at all frequencies ν) whose flipping slightly increases the energy. Their cumulative effect is responsible for the energy difference between replicas, which smoothly grows moving away from the ground state.

B. Slashdot and competing valleys of near-optimal balance

For Slashdot, the low-energy landscape is markedly different: distinct peaks in the Hamming distances are clearly visible (Fig. 2) and are related to the three valleys observed in the energy histogram of Fig. 1(b). In fact, a scatter plot [Fig. 5(a)] reveals that while the two valleys at higher energy are nearby also in configuration space [cloud of points in the down-left corner in Fig. 5(a)] both of them are far away from the lowest valley (points in the upper-right corner). To confirm that indeed this multivalley profile is not due to undersampling of the low-energy landscape, the search for replicas in $[\delta_{up}, \delta_{up} + \epsilon]$ was performed a large number of times (compare the two values of r in Table II). Even increasing tenfold r no new valley emerged for this network.

Looking at the spin frequencies of Slashdot [Fig. 3(b)] we can also observe a feature absent in Epinions, namely the presence of three sharp spikelike peaks for $z(\nu)$. If broad peaks usually contain small connected components, sharp, spikelike peaks in the plot of $z(\nu)$ are more likely to be associated to large connected components whose spins are simultaneously flipped in some of the replicas. A thorough analysis reveals that these three peaks correspond in fact to three connected subnetworks characterized by a high level of internal balance, higher than with the rest of the network. In Table IV we report some features of the corresponding subnetworks and in Fig. 6 we draw their adjacency matrices and graphs. These subnetworks are responsible for the formation of competing valleys of near-optimal balance described earlier. In fact, while the internal arrangement of their spins is usually frozen on each valley, their relative orientation with respect to the rest of the network may change passing from one valley to another, meaning that all spins of a subnetwork are simultaneously flipped; see Fig. 5(c). Computing a few sample trajectories from one valley to another [Fig. 5(b)], we can observe the presence of an energy barrier: the paths break the internal balance of some of the

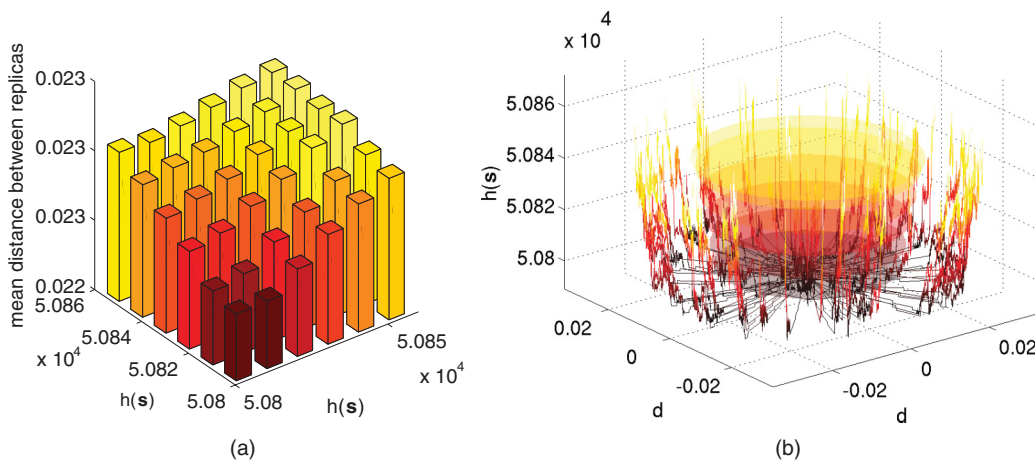


FIG. 4. (Color online) Epinions. (a) Distance among replicas vs energy of a replica. The replicas of Fig. 1(a) are binned into six bins according to their energy, and the mean of the relative Hamming distances is computed. The vertical axis [and color (gray) code] represents the mean over bins of the relative distances. The replicas of least energy are also closer, and the distance grows regularly with the energy. (b) Sample minimal energy paths connecting the global and a local minimum. For visualization purposes, the trajectories are depicted as radially distributed according to a polar coordinate, with the global optimum placed in the origin. The vertical axis [and color (gray) code] represents the energy. The radius of the disks represent the average distance among the replicas in correspondence of the six bins of (a). The horizontal parts on the paths correspond to isoenergetic flips.

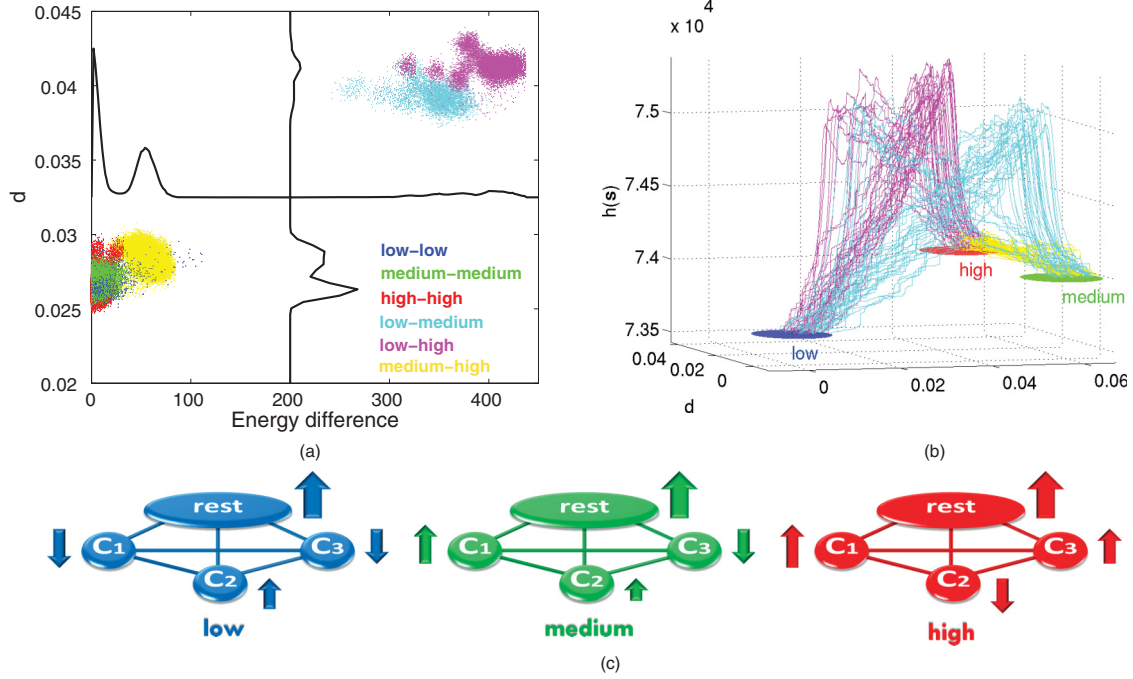


FIG. 5. (Color online) Slashdot. (a) Three valleys of minima corresponding to the three peaks in Fig. 1(b) are called low, medium, and high, according to their energy. For each pair of minima $s^{(i)}$ and $s^{(j)}$, the scatter plot shows differences in energy $|h(s^{(i)}) - h(s^{(j)})|$ versus the relative Hamming distance d for both intra and intervalley peaks. The two valleys medium and high are near and both more distant from the low valley. (b) A few sample trajectories connecting minima in different valleys. The radius of the trajectories corresponds to the average intravalley distance among the replicas. The height of the trajectories is indicative of the energy barrier between the valleys. To improve readability, the degenerate spin flips are not shown. (c) The three internally balanced communities C_i (described in Tables IV and V and Fig. 6) and their average magnetization in the three valleys of near-optimal balance.

subnetworks before they are able to rearrange them again in another manner. In terms of our social networks, the formation of different valleys of near-optimal balance means the presence of possible alternative “alliances” between the majority of the users and a few internally balanced subnetworks of users (not necessarily mutually friends among them). Fixing the relationship with one such subnetwork constrains the sign of the relationship with the other subnetworks. Different arrangements lead to slightly different global levels of balance for the whole network.

As already mentioned, a necessary condition for the spins of a subnetwork to have constant sign relative to each other

in all low-energy replicas (which means also to be flipped simultaneously in all these near-optimal configurations) is that the subnetwork has to have a high level of balance internally, and a certain amount of frustration with respect to the rest of the network. At low energies, in fact, this favors a constant choice of spin orientation within the subnetwork which can, however, vary from valley to valley.

Denote C_1, C_2 , and C_3 the three subnetworks of Table IV (and $rest$ their complement in the original signed graph). By lumping together all nodes of each subnetwork, the corresponding matrix of adjacencies (blocks ordered as C_1, C_2, C_3 , and $rest$) is the following:

$$A = \begin{bmatrix} 2807 & 16 & -206 & -129 \\ 16 & -96 & -1 & -19 \\ -206 & -1 & -190 & -359 \\ -129 & -19 & -359 & 242654 \end{bmatrix}, \quad (4)$$

where the original amounts of positive and negative edges are $A(+/-)$

$$= \begin{bmatrix} 4169/1362 & 30/14 & 21/227 & 6217/6346 \\ 30/14 & 11/107 & 0/1 & 113/132 \\ 21/227 & 0/1 & 7/197 & 422/781 \\ 6217/6346 & 113/132 & 422/781 & 345510/102856 \end{bmatrix}. \quad (5)$$

Both C_2 and C_3 have a vast majority of internal negative edges, see Fig. 6 and Table IV. In correspondence of the optimal balance, the gauge transformed adjacency matrix for

TABLE IV. Slashdot balanced subnetworks: nodes and edges of the three subgraphs C_i identified from Fig. 3. The row $rest$ denotes the complement to the C_i in \mathcal{J} . Internal edges are those connecting two nodes of the same C_i , while external nodes are those connecting a node in C_i and one in C_j (or in $rest$). The C_i are visualized in Fig. 6.

Subnetwork	Nodes n_{C_i}	Edges			
		+1 int.	-1 int.	+1 ext.	-1 ext.
C_1	855	4169	1362	6268	6587
C_2	62	11	107	143	148
C_3	58	7	197	443	1009
$rest$	51073	345510	102856	6752	7259

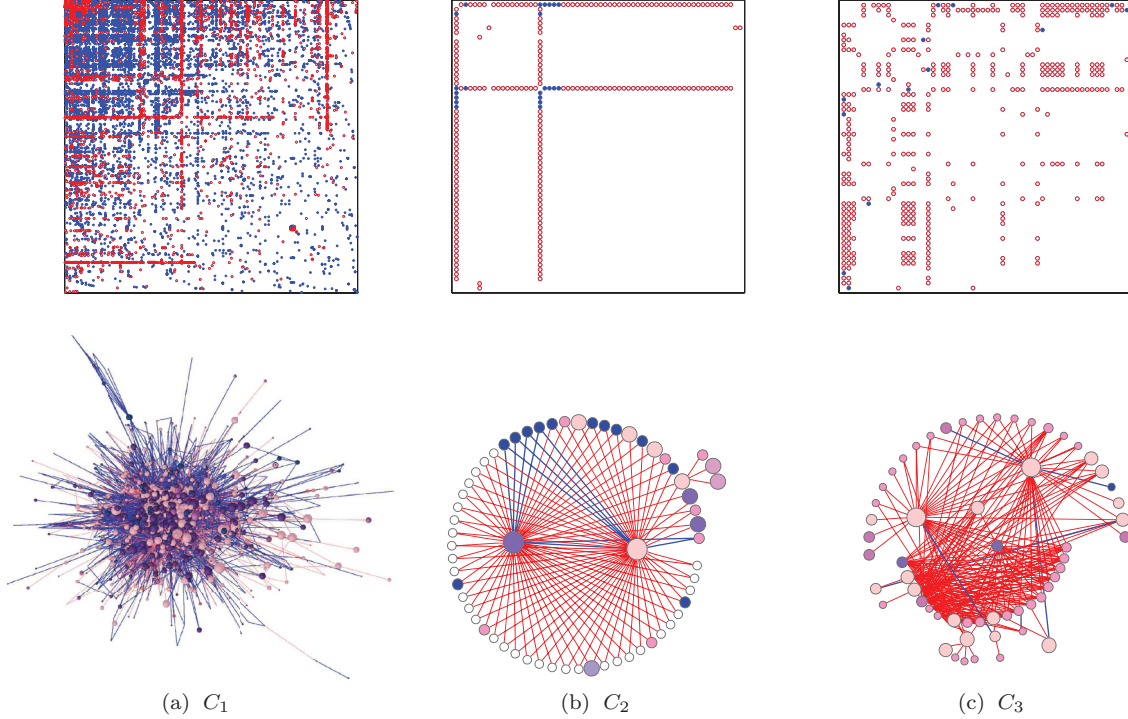


FIG. 6. (Color online) Slashdot: the three internally balanced subnetworks C_1 , C_2 , and C_3 of Table IV. The adjacency matrices (first row) and the corresponding signed graphs (second row) are shown. Blue (full) dots correspond to +1 edges, red (empty) to -1. In the corresponding graph, blue (thick) lines correspond to +1 edges, red (thin) lines to -1. The color code for the nodes reflects the sum of the external edges: blue (darker) means positive sum, red (lighter) negative, and white no external edges.

the subnetworks is

$$\mathcal{A}_\sigma(+/-) = \begin{bmatrix} 5441/90 & 32/12 & 242/6 & 6726/5837 \\ 32/12 & 118/0 & 1/0 & 170/75 \\ 242/6 & 1/0 & 204/0 & 809/394 \\ 6726/5837 & 170/75 & 809/394 & 381167/67199 \end{bmatrix},$$

where it can be observed that the various C_i have very few residual negative edges (in particular C_2 and C_3 have none), meaning that indeed these subnetworks are internally balanced. If we look at the structure of the adjacency matrices of the C_i in Fig. 6, it is easy to understand why so many negative edges disappear in the gauge transformed \mathcal{A}_σ : the negative edges are all in correspondence of the same users. This is particularly visible in the adjacency matrix of C_1 : each row or column is highly skewed towards positive or negative edges. Such skewed sign distributions are the trademark for “apparent disorder,” i.e., negative edges which can be eliminated by means of gauge transformations and hence that do not spoil global balance. In Slashdot, users with a high number of negative edges are known as trolls [20]. Trolls do not add tension to the network, as they are unanimously tagged as foes by the other users. Looking carefully at Fig. 6 it is possible to observe that the subnetworks C_2 and C_3 , where negative edges are the vast majority, have nevertheless all positive cycles. In C_2 all cycles have length 3 and pass through the (positive) edge linking the two highly connected nodes. In C_3 , instead, cycles have length 4 and are composed of four negative edges.

Observing the pattern of signs (and sign flips) of the C_i in the 5557 low-energy replica of Slashdot, a high degree of regularity can be seen. Call $\mathbf{s}_{C_i}^{(j)}$ the spin configuration of the C_i subnetwork in the j th low-energy replica, and n_{C_i} the number of spins of C_i . By construction, the relative Hamming distance within the subnetwork

$$d(\mathbf{s}_{C_i}^{(j)}, \mathbf{s}_{C_i}^{(k)}) = [1 - (\mathbf{s}_{C_i}^{(j)})^T \mathbf{s}_{C_i}^{(k)} / n_{C_i}] / 2$$

is always zero. The intervalley relative Hamming distance is shown in Fig. 5(a). The “average magnetization” within a subnetwork and within a valley is computed restricting the computation to the \mathbf{s}_{C_i} spins and to the replicas falling into the valley. If r_{low} is the number of replicas in the low valley, then the average magnetization for the low valley is

$$\langle \mathbf{s}_{C_i} \rangle_{\text{low}} = \sum_{k \in C_i} \sum_{j \in \text{low}} s_k^{(j)} / (r_{\text{low}} n_{C_i}),$$

and similarly for $\langle \mathbf{s}_{C_i} \rangle_{\text{medium}}$ and $\langle \mathbf{s}_{C_i} \rangle_{\text{high}}$, $i = 1, 2, 3$. These average magnetizations are shown in Fig. 5(c) and Table V. It can be observed that for example the spins \mathbf{s}_{C_1} are flipped passing from the low energy valley to the medium-high energy valleys. These community-wide flips do not modify the intravalley energy, but they alter the energy of the cut set between the C_i 's and with the rest of the network. The increase in energy passing from one valley to another is a consequence of these changes. The cut sets between C_1 and C_2 and between C_2 and C_3 are always negligible, while the cut set between C_1 and C_3 can increase the energy considerably. This happens when $\langle \mathbf{s}_{C_1} \rangle$ and $\langle \mathbf{s}_{C_3} \rangle$ are not solidary, i.e., in the medium valley. This makes the most of the difference in

TABLE V. Slashdot valleys: $\langle s_{C_i} \rangle_{\text{low, medium, high}}$ is the average magnetization of the subnetwork C_i (or of *rest*) in the three low-energy valleys of Fig. 5.

$\langle s_{C_i} \rangle$	Valley		
	low	medium	high
C_1	-0.712	0.712	0.712
C_2	0.513	0.066	-0.663
C_3	-0.517	-0.517	0.506
<i>rest</i>	0.797	0.804	0.807

energy between low and medium valleys. In the high valley, instead, the magnetizations $\langle s_{C_1} \rangle_{\text{high}}$ and $\langle s_{C_3} \rangle_{\text{high}}$ are again aligned. However, both are flipped with respect to the low valley, and this reflects in the changes of energies in the cut sets relative to the *rest* of the network. Remember that *rest* contains a very large fraction of the network, and that it is highly

biased towards positive magnetization (see Table V), which is essentially uninfluenced by flipping of small communities. Nevertheless, the internal rearrangements inside *rest* due to the flips of s_{C_1} and s_{C_3} induce a consistent increase of frustration within *rest*. In summary, it appears that a feature instrumental to the creation of separated energy valleys is the presence of perfectly balanced subnetworks (like C_2 , C_3 and, to a large extent, also C_1). These can be composed of friends as well as of “declared” enemies: for what concerns structural balance, the trolls of C_2 and C_3 play exactly the same role as the users having many positive edges.

V. FINAL CONSIDERATIONS

The point of view taken in this paper, identify a signed social network with a spin glass (both are signed graphs), allows one to pass from a local viewpoint of pairwise relationships between individuals to a global perspective of organization

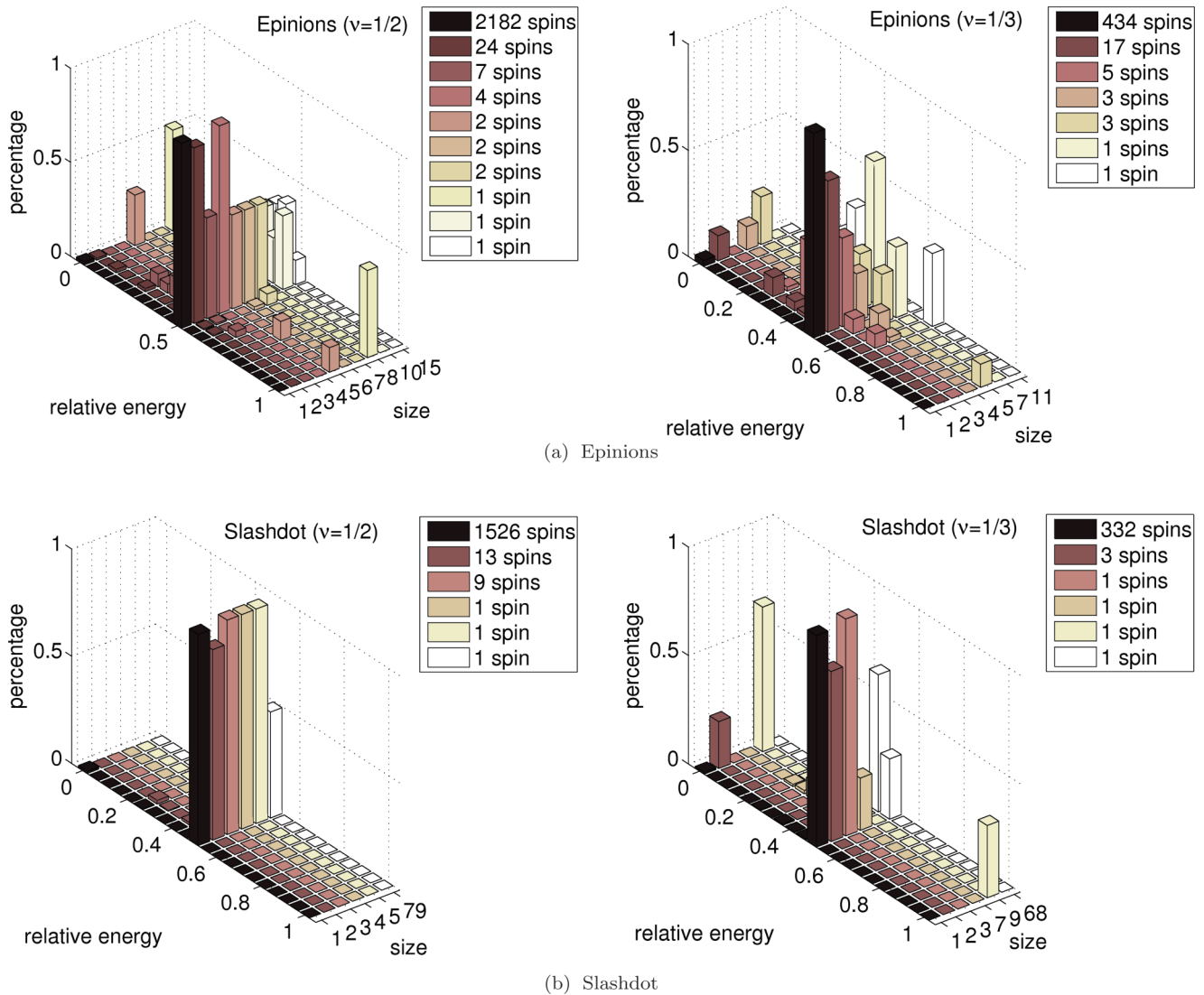


FIG. 7. (Color online) Relative energy of the motifs flipping with frequencies $\nu = 1/2$ and $\nu = 1/3$. These motifs are grouped according to their size. The gray scale (color online) represents their number. In all histograms the relative energy (energy through the cut set divided by the corresponding number of edges) is concentrated around 0.5, meaning that half of the edges are frustrated in the ground state. Therefore, the peaks at $\nu = 1/2$ and $\nu = 1/3$ contain mostly isoenergetic motifs. These are described in Tables VI and VII.

of the signs in a given social network. A by-product of the approach is that a wide range of concepts developed for spin glasses can be used to investigate social networks. These include a “natural” energy functional whose global optimum corresponds to the value of structural balance in the network, a direct identification of frustration with the “social stress” at the basis of unbalance, and the possibility of evaluating near-optimal possible arrangements using the tools developed for the rough energy landscapes of disordered systems.

It is worth mentioning that one aspect which cannot be studied with these tools is the clustering of a social network into communities of friends [22]. In this case the communities are identified by the nodes of the subgraphs connected by + edges, and are separated by - edges. As soon as the system is not globally balanced, the number of such clusters is certainly larger than 2, hence the bipartition associated to an Ising spin is not enough for exact clustering (in fact the subnetworks discussed for Slashdot are balanced subgraphs, not communities of friends). See [23,24] for more details and pointers to the literature on these clustering methods. It is not clear to us if more complex models of spin glasses, with more than two states (e.g., Potts models), can be used for this scope.

The possibility of exploring the low-energy landscape of the equivalent Ising model of large signed social networks is an important tool for investigating some peculiarities of the social interactions which take place inside these communities. In the paper we have presented examples of what can be achieved using a large number of low energy minima for the characterization of two large-scale on-line networks, Epinions and Slashdot.

In spite of a similar fraction of negative edges in the two networks (16.5% for Epinions and 23.9% for Slashdot) and of a similar low level of frustration (partially ferromagnetic behavior), two quite different low-energy landscapes have been identified: a single valley for Epinions and a set of three competing valleys for Slashdot. We associate this different qualitative behavior with the presence of exactly balanced (and highly connected) subnetworks, whose internal balance must be destroyed and reformed in order to pass from one valley to another. It is precisely the presence of these balanced subnetworks (and their arrangement with the rest of the network) that leads to a partial breaking of ergodicity in the system, and to the creation of energy barriers between competing near-optimal valleys. It is worth observing that these subnetworks are not necessarily composed by friends, making the determination of energy barriers like these a difficult task if one simply looks at the sign distributions on the edges and subdivides the nodes into clusters.

These results represent a clear demonstration that, for complex systems like large social networks, global properties cannot be inferred by local or mean features: more sophisticated analytical and computational tools must be developed and applied.

ACKNOWLEDGMENTS

C.A. acknowledges financial support from MIUR (Ministero dell’Istruzione, dell’Università e della Ricerca) and

INdAM (Istituto Nazionale di Alta Matematica). The EU-IndiaGRID2 project (European FP7 e-Infrastructure Grant No. 246698) is acknowledged for the use of its grid infrastructure.

APPENDIX: ISOENERGETIC MOTIFS

Both the peaks at $\nu = 1/2$ and $\nu = 1/3$ described in Fig. 3 contain a large number of small disconnected components. For the two networks, the vast majority of these connected components are isoenergetic. In Fig. 7 these correspond to motifs having relative energy e^{rel} through the cut set equal to 0.5, where the relative energy of each motif \mathcal{M} is computed as the energy through the cut set that isolates the motif from the rest of the network, divided by the number

TABLE VI. Isoenergetic motifs identified under the peak at $\nu = 1/2$. The values c_i^+ and c_i^- refers to the number of positive and negative edges from the i th node to the rest of the network in the gauge transformed \mathcal{J}_σ . The motifs are classified according to their size and then to the size of the cut set with the rest of the network. In the case marked with the asterisk, one of the triangles on the top presents a frustration. The pictures reported in the table represent examples of the corresponding motifs: thick line indicates a positive edge, thin line a negative edge.

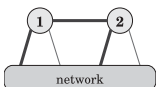
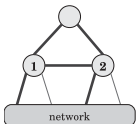
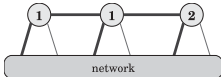
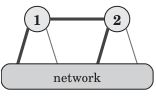
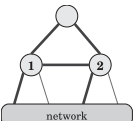
Motif \mathcal{M}	c_1^+	c_1^-	c_2^+	c_2^-	Epinions	Slashdot
	1	1	-	-	1928	1469
	2	2	-	-	180	155
	3	3	-	-	40	41
	4	4	-	-	15	14
	5	5	-	-	6	6
	6	6	-	-	2	6
	7	7	-	-	1	2
	8	8	-	-		3
	9	9	-	-		2
	17	17	-	-		
	24	24	-	-		
1 node	Total				2172	1698
	1	1	1	1	13	5
	1	1	2	2	5	2
	1	1	3	3	2	2
	1	1	4	4	1	1
	1	1	5	5	2	
	2	2	2	2	1	1
	2	2	3	3		1
2 nodes	Total				24	12
	1	1	0	0	2	4*
	2	2	0	0		2
	4	4	0	0	1	
	1	1	1	1	1	2
	1	1	2	2		1
3 nodes	Total				4	9

TABLE VII. Isoenergetic motifs identified under the peak at $\nu = 1/3$. The c_i^+ and c_i^- are the positive and negative edges of the i th node through the cut set separating a motif from the rest of the network in the ground state. In the case marked with a double asterisk the two nodes are interconnected by a negative edge. The pictures reported in the table represent examples of the corresponding motifs: thick line indicates a positive edge, thin line a negative edge.

Motif \mathcal{M}	c_1^+	c_1^-	c_2^+	c_2^-	Epinions	Slashdot
	1	1	-	-	367	245
	2	2	-	-	51	53
	3	3	-	-	17	13
	4	4	-	-	2	6
	5	5	-	-	1	
	6	6	-	-	1	1
	9	9	-	-	1	
	15	15	-	-	1	
	17	17	-	-	1	
	20	20	-	-	1	
1 node	Total				442	318
	1	1	1	1	2	
	1	1	2	2	1	
	1	1	3	3	2	
	2	2	3	3		1
	1	0	0	1	3	1
	2	1	0	1	1	
	1	0	0	1		1**
2 nodes	Total				9	3
	1	0	0	1	1	1
3 nodes	Total				1	1

of edges in the cut set itself:

$$e_{\mathcal{M}}^{\text{rel}} = \sum_{\substack{i \in \mathcal{M} \\ j \notin \mathcal{M}}} (1 - J_{ij} s_i s_j) / \left(2 \sum_{i \in \mathcal{M}} c_i \right),$$

with c_i the connectivity through the cut set of the i th node of the motif \mathcal{M} (c_i^+ and c_i^- are the corresponding numbers of +1 and -1 edges of c_i). Hence $e_{\mathcal{M}}^{\text{rel}} = 0$ means that with respect to the ground state the motif \mathcal{M} has all “satisfied” edges across the cut set, $e_{\mathcal{M}}^{\text{rel}} = 0.5$ means it has 50% of frustrated edges, and $e_{\mathcal{M}}^{\text{rel}} = 1$ means 100% of edges frustrated. A catalog of the isoenergetic motifs under the two peaks is given in Tables VI and VII.

While the presence of isoenergetic motifs under the $\nu = 1/2$ peak is straightforward to explain, the abundance of such motifs under the $\nu = 1/3$ peak is less obvious and requires an extra bit of investigation. On what follows we restrict ourselves to the size-1 isoenergetic motifs of Epinions (in this case the motif \mathcal{M} is represented and indicated by its only node i). For each low energy replica σ (with the relative gauge-transformed adjacency matrix \mathcal{J}_σ) and for each node i (size-1 isoenergetic motif under either the peak at $\nu = 1/2$ or that at $\nu = 1/3$) we calculate the percentage of edges which change sign with

respect to the initial matrix \mathcal{J} . This value is given by the ratio

$$\bar{\rho}(\sigma, i) = \frac{\|\mathcal{J}_\sigma^{(i,\cdot)} - \mathcal{J}^{(i,\cdot)}\|_1}{2\|\mathcal{J}^{(i,\cdot)}\|_1},$$

where $\mathcal{J}^{(i,\cdot)}$ represents the i th row of the matrix and $\|\cdot\|_1$ the 1-norm. We can easily attribute a plausible meaning to some of the values that this ratio can assume, as follows:

(i) $\bar{\rho}(\sigma, i) = 0$: the gauge transformation σ flips neither node i nor its neighbors.

(ii) $\bar{\rho}(\sigma, i) = 1/2$: the gauge transformation σ flips only half (mostly one) of the neighbors of node i .

(iii) $\bar{\rho}(\sigma, i) = 1$: the gauge transformation σ flips the node i (or, less likely, all its neighbors).

In order to compare two differently populated peaks at $\nu = 1/2$ and $\nu = 1/3$, for each σ we must normalize the counts for the three cases:

$$\rho_0(\sigma) = \frac{N_0}{N}, \quad \rho_{1/2}(\sigma) = \frac{N_{1/2}}{N}, \quad \rho_1(\sigma) = \frac{N_1}{N},$$

where N_k is the number of i such that $\bar{\rho}(\sigma, i)$ is equal to k and $N = \sum_k N_k$. As most pairs (σ, i) are such that $\bar{\rho}(\sigma, i)$ assume the values 0, 1/2, or 1, we have the “empirical” constraint:

$$\rho_0(\sigma) + \rho_{1/2}(\sigma) + \rho_1(\sigma) \approx 1 \quad \forall \sigma. \quad (\text{A1})$$

The comparison of the values obtained for Epinions is shown in Fig. 8. For ρ_1 (bottom panel) the plots at $\nu = 1/2$ and at $\nu = 1/3$ almost totally overlap. The top plot for ρ_0 which, as already mentioned, refers to both node and neighboring nodes unchanged in a replica, instead shows a systematic difference (less frequent in $\nu = 1/3$ than in $\nu = 1/2$). From Eq. (A1),

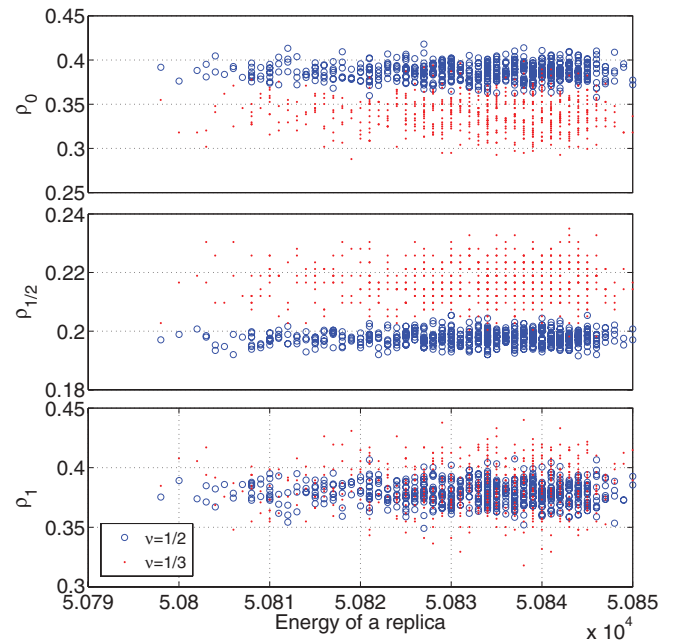


FIG. 8. (Color online) Epinions: origin of the size-1 motifs for $\nu = 1/2$ and $\nu = 1/3$. Plots of the ρ_0 , $\rho_{1/2}$, and ρ_1 ratios for the 2172 isoenergetic size-1 motifs identified under the peak at $\nu = 1/2$ (circles) and for the 442 size-1 isoenergetic motifs belonging to the peak at $\nu = 1/3$ (points). The case $\rho_{1/2}$ (referring to gauge transformations that change 50% of the edges through the cut set) is more frequent under the $\nu = 1/3$ peak than under the $\nu = 1/2$ one.

such a difference is compensated by an equal but opposite difference in the middle panel for $\rho_{1/2}$. Recalling that $\rho_{1/2}$ refers to the case in which 50% of the neighboring nodes of node i are flipped, then we can conclude that the peak at $\nu = 1/3$ appears

to be due, at least to some extent, to a bulk of the network which is less “rigid” than under the $\nu = 1/2$ peak and hence allows for more frequent internal rearrangements. It is worth noting that this behavior is uniform across all low-energy replicas.

-
- [1] T. Antal, P. L. Krapivsky, and S. Redner, *Phys. Rev. E* **72**, 036121 (2005).
- [2] G. Facchetti, G. Iacono, and C. Altafini, *Proc. Natl. Acad. Sci. USA* **108**, 20953 (2011).
- [3] S. Galam, *Physica A: Stat. Theor. Phys.* **230**, 174 (1996).
- [4] K. Kulakowski, *Comput. Sci. Eng.* **9**, 80 (2007).
- [5] S. A. Marvel, S. H. Strogatz, and J. M. Kleinberg, *Phys. Rev. Lett.* **103**, 198701 (2009).
- [6] A. Srinivasan, *Proc. Natl. Acad. Sci. USA* **108**, 1751 (2011).
- [7] M. Szell, R. Lambiotte, and S. Thurner, *Proc. Natl. Acad. Sci. USA* **107**, 13636 (2010).
- [8] F. Heider, *J. Psych.* **21**, 107 (1946).
- [9] D. Cartwright and F. Harary, *Psych. Rev.* **63**, 277 (1956).
- [10] G. Toulouse, *Commun. Phys.* **2**, 115 (1977).
- [11] D. C. Mattis, *Phys. Lett. A* **56**, 421 (1976).
- [12] K. Binder and A. P. Young, *Rev. Mod. Phys.* **58**, 801 (1986).
- [13] O. C. Martin, in *New Optimization Algorithms in Physics*, edited by A. K. Hartmann and H. Rieger (Wiley-VCH, Weinheim, 2005).
- [14] A. K. Hartmann and H. Rieger, *Optimization Algorithms in Physics* (Wiley-VCH, Berlin, 2001).
- [15] J. Leskovec, D. Huttenlocher, and J. Kleinberg, in *ACM SIGCHI Conference on Human Factors in Computing Systems* (ACM SIGCHI, Atlanta, GA, 2010).
- [16] G. Iacono, F. Ramezani, N. Soranzo, and C. Altafini, *IET Syst. Biol.* **4**, 223 (2010).
- [17] M. Mezard, G. Parisi, and M. Virasoro, *Spin Glass Theory and Beyond* (World Scientific, Singapore, 1986).
- [18] R. Guha, R. Kumar, P. Raghavan, and A. Tomkins, in *Proceedings of the 13th International Conference on World Wide Web* (Association for Computing Machinery, New York, 2004), pp. 403–412.
- [19] C. A. Lampe, E. Johnston, and P. Resnick, in *Proceedings of the SIGCHI Conference on Human Factors in Computing Systems* (Association for Computing Machinery, New York, 2007), pp. 1253–1262.
- [20] J. Kunegis, A. Lommatzsch, and C. Bauckhage, in *Proceedings of the 18th International World Wide Web Conference* (Association for Computing Machinery, New York, 2009), pp. 741–750.
- [21] S. Kirkpatrick, *Phys. Rev. B* **16**, 4630 (1977).
- [22] J. A. Davis, *Human Relat.* **20**, 181 (1967).
- [23] P. Doreian and A. Mrvar, *Social Netw.* **18**, 149 (1996).
- [24] S. Wasserman and K. Faust, *Social Network Analysis: Methods and Applications* (Cambridge University Press, Cambridge, UK, 1994).